# Automated TEM-based Quantitative Analysis of Etioplast Morphology


Submitted By

**Md. Nashir Kazi**

**ID: 221-35-938**

**Department of Software Engineering**

**Daffodil International University**

Supervised By

**Mr. MD. Shohel Arman**

**Assistant Professor**

**Department of Software Engineering**

**Daffodil International University**


A thesis submitted in partial fulfillment of the requirement for the degree of Bachelor of Science in Software Engineering

Fall 2025

## APPROVAL

This thesis titled on "**Automated TEM-Based Quantitative Analysis of Etioplast Morphology**", submitted by **MD. NASHIR KAZI (ID: 221-35-938)** to the Department of Software Engineering, Daffodil International University has been accepted as satisfactory for the partial fulfillment of the requirements for the degree of Bachelor of Science in Software Engineering and approval as to its style and contents.

### BOARD OF EXAMINERS

---

**Chairman**

**Dr. Imran Mahmud**
**Professor & Head**
Department of Software Engineering
Faculty of Science and Information Technology Daffodil International University

---

**Internal Examiner 1**

**Afsana Begum**
**Assistant Professor**
Department of Software Engineering
Faculty of Science and Information Technology
Daffodil International University

---

**Internal Examiner 2**

**Md. Shohel Arman**
**Assistant Professor**
Department of Software Engineering
Faculty of Science and Information Technology
Daffodil International University

---

**Internal Examiner 3**

**Nadira Islam**
**Assistant Professor**
Department of Software Engineering
Faculty of Science and Information Technology
Daffodil International University

---

**External Examiner**

**Md Manowarul Islam**
**Professor**
Department of Computer Science and Engineering
Jagannath University, Bangladesh

## DAFFODIL INTERNATIONAL UNIVERSITY

**DECLARATION OF THESIS AND COPYRIGHT**

| | | |
|---|---|---|
| Author's Full Name | : | MD NASHIR KAZI |
| Date of Birth | : | 31 December, 2000 |
| Title | : | Automated TEM-based Quantitative Analysis of Etioplast Morphology |
| Academic Session | : | Fall 2025 |

I declare that this thesis is classified as:

| | | |
|---|---|---|
| ☐ | CONFIDENTIAL | (Contains confidential information under the Official Secret Act 1997)* |
| ☐ | RESTRICTED | (Contains restricted information as specified by the organization where research was done)* |
| ☐ | OPEN ACCESS | I agree that my thesis to be published as online open access (Full Text) |

I acknowledge that Daffodil International University reserves the following rights:

1. The Thesis is the Property of Daffodil International University.
2. The Library of Daffodil International University has the right to make copies of the thesis for the purpose of research only.
3. The Library of Daffodil International University has the right to make copies of the thesis for academic exchange.

Certified by:

Nashir

_____
(Student's Signature)

221-35-938
_____
Student ID
Date:

_____
(Supervisor's Signature)

Mr. Md. Shohel Arman
_____
Name of Supervisor
Date:

## SUPERVISOR’s DECLARATION

I hereby declare that I have checked this thesis and, in my opinion, this thesis is adequate in terms of scope and quality for the award of the degree of Bachelor of Science

_____

(Supervisor’s Signature)

Full Name : Mr. Md. Shohel Arman

Position : Assistant Professor

Date : 27 November, 2025

## STUDENT'S DECLARATION

I hereby declare that the work in this thesis is based on my original work except for quotations and citations which have been duly acknowledged. I also declare that it has not been previously or concurrently submitted for any other degree at Daffodil International University or any other institution.

_____

(Student's Signature)

Full Name : MD. NASHIR KAZI

ID Number : 221-35-938

Date : 27 November, 2025

# Automated TEM-based Quantitative Analysis of Etioplast Morphology

MD. NASHIR KAZI

Thesis submitted in fulfillment of the requirements
for the award of the degree of
Bachelor of Science

Department of Software Engineering (Major in Data Science)

DAFFODIL INTERNATIONAL UNIVERSITY

November, 2025

# Acknowledgement

First and foremost, I am sincerely grateful to Almighty Allah for granting me the strength, patience, and good health to see this final-year thesis through to completion. Without His blessings, none of this would have been possible.

I would like to express my heartfelt gratitude to my supervisor, **Mr. Md. Shohel Arman,** Assistant Professor, Department of Software Engineering, Daffodil International University, for his constant guidance and support. From helping me refine the topic to reviewing my experiments and writings, his feedback and encouragement have been invaluable. His patience and willingness to help at every stage made this journey much easier and more meaningful for me.

I am also deeply thankful to Dr. Salek Ahmed Sajib, Postdoctoral Researcher at the French National Centre for Scientific Research (CNRS). His support with the TEM etioplast dataset and his deep expertise in plastid biology significantly strengthened the scientific side of this work. His explanations and insights about etioplasts and plastid ultrastructure helped me truly understand the biological concepts behind the images and connect them properly with the computational and automation aspects of the thesis.

I am grateful to all the respected teachers and staff of the Department of Software Engineering, Daffodil International University. Their teaching, advice, and continuous support over the years have built the foundation of my technical knowledge and research skills, without which this work would not have been possible.

Finally, I would like to thank my parents, family members, and friends for their endless love, patience, and prayers. Their encouragement during stressful moments, as well as their belief in me, has always been my greatest source of strength and motivation throughout this journey.

 

## Abstract

Etioplasts are plastids that develop in dark grown tissues and later convert into chloroplasts when exposed to light. Their internal ultrastructure made up of the prolamellar body (PLB), prothylakoids (PTs), plastoglobules and occasional starch grains contains important information about plastid development, stress responses and genetic changes. Transmission electron microscopy (TEM) is the gold standard for visualising these nanostructures, but quantitative analysis still depends largely on manual tracing in tools such as ImageJ/Fiji. This makes large scale studies slow, subjective and difficult to reproduce. This thesis presents an automated framework for quantitative analysis of etioplast ultrastructure from TEM micrographs. TEM images of *Arabidopsis thaliana* dark grown seedlings, acquired in collaboration with a CNRS laboratory, are manually annotated and then validated by a plastid expert to obtain high quality ground truth masks for etioplast envelopes, PLBs, PTs, plastoglobules and starch grains. After standardised preprocessing and data augmentation, these annotations are used to train YOLO based instance segmentation models (YOLOv5-seg, YOLOv8-seg and YOLOv12-seg). The best performing model is exported as a .pt checkpoint and integrated into a server side pipeline that accepts new TEM images via an API, runs inference and extracts morphometric descriptors such as etioplast and PLB area, PT number and total length, plastoglobule count and plastoglobule diameter. All measurements are stored in structured CSV or JSON files for downstream analysis. A lightweight generative AI module then operates only on these numeric outputs, producing short, human-readable summaries without altering any underlying measurements. The system is evaluated using standard segmentation metrics (Dice, IoU, precision, recall), parameter accuracy measures against expert annotations (MAE, RMSE, MAPE, Bland Altman analysis) and qualitative expert review. Overall, the results indicate that modern segmentation models, combined with explicit calibration and quality control, can turn TEM-based etioplast analysis from a manual, artisanal procedure into a reproducible and scalable quantitative pipeline


 

## Table Of Contents



 

## Table Of Figures



 

# Chapter 1

# Introduction

## 1.1 Background

Plastids are central, multifunctional organelles in plant cells, responsible not only for photosynthesis but also for lipid biosynthesis and the production of a wide range of primary and secondary metabolites that support growth, development and stress adaptation [5]. In dark-grown tissues, chloroplasts do not develop directly. Instead, plastids differentiate into etioplasts, a non-photosynthetic, transitional state that can be rapidly converted into functional chloroplasts once the seedling is exposed to light [6]. Etioplasts display a characteristic internal architecture consisting of a three dimensional prolamellar body (PLB), connected prothylakoid membranes (PTs), lipid-rich plastoglobules and, in some genotypes or conditions, starch grains [7], [8]. The relative size, organisation and abundance of these substructures are closely linked to chloroplast biogenesis, the molecular composition of the inner membranes and the way plants respond to genetic perturbations and environmental or chemical stressors [20], [21].Transmission electron microscopy (TEM) remains the gold-standard technique for visualising such micrometer-scale plastid features. Ultrathin sections of chemically fixed and stained tissue are imaged at high accelerating voltage, producing high-contrast micrographs in which membranes, PLBs and protein-rich regions appear darker than the surrounding stroma [9], [11]. In etioplast research, TEM and electron tomography have been used to resolve the three-dimensional lattice of the PLB, its transformation into thylakoid stacks during de etiolation and the subtle ultrastructural changes induced by pigment mutants or altered membrane protein composition [9]. Similar TEM based workflows underpin quantitative analyses of chloroplast grana morphology, where precise measurements of membrane dimensions and stacking are essential for linking structure to function [10].Despite these advances in imaging, the downstream analysis of etioplast ultrastructure is still dominated by manual or semi-manual measurements in general purpose tools such as ImageJ or Fiji. In many studies, researchers select a limited number of plastids, trace PLBs, PTs and plastoglobules by hand, and then extract a small set of areas, lengths or shape descriptors from these tracings [20]. This process is labor-intensive and subjective, making it difficult to scale to larger datasets or to ensure that different analysts, laboratories or studies apply the same criteria in a reproducible way [21]. As a result, the statistical power of etioplast studies is often constrained by small sample sizes, and meaningful comparison across genotypes, treatments and experiments becomes challenging. Recent AI-assisted tools such as GRANA, developed for chloroplast grana morphometry, illustrate how hybrid intelligence can accelerate and standardize ultrastructural analysis [10], but comparable, task-specific solutions for etioplasts and their PLB/PT networks are still lacking, motivating the development of automated, quantitative pipelines in this domain.

 

## 1.2 Motivation

Over the past decade, deep learning has changed how images are analyzed in medicine, biology and many other fields. Convolutional neural networks (CNNs) and encoder decoder architectures such as U-Net can learn to segment complex structures directly from pixel data when suitable training annotations are available [1]. Single stage detectors such as the YOLO family extend this idea to instance segmentation, predicting class labels, bounding boxes and pixelwise masks in a single forward pass. In parallel, modern software frameworks and web technologies now make it practical to deploy trained models as web applications that run in a browser, so that users interact with a simple graphical interface rather than with GPUs and Python code [10]. Despite these advances, there is still no dedicated, openly described system for automated quantitative analysis of etioplast ultrastructure [21]. Plant biologists who study etiolation, de-etiolation or plastid mutants therefore continue to rely on manual tracing to measure PLB area, total prothylakoid length or plastoglobule size distributions in TEM images [7]. This gap motivates the development of an integrated pipeline that starts from raw TEM micrographs and ends with calibrated, reproducible morphometric features that can be used directly for biological interpretation and statistical analysis [10].

## 1.3 Problem Statement

Conventional TEM workflows for etioplast analysis face three main limitations. First, the segmentation of key structures (etioplast envelope, PLBs, PTs, plastoglobules and starch) is usually done manually or only partially automated. This introduces subjective bias, depends strongly on the experience of the analyst, and severely limits how many cells can be analyzed in a single study [7]. Second, even when structures are segmented, there is no widely adopted and standardised way to convert masks into calibrated areas, lengths and counts while properly handling pixel to nanometer calibration and basic measurement uncertainty. Different studies often apply their own measurement rules, which makes it difficult to compare results or perform meta-analyses [11]. Third, there is a lack of accessible software that brings the full analysis pipeline together in a consistent, user friendly tool for plant biologists. Existing scripts are often written for a single project, remain undocumented and are rarely shared, so published findings are hard to reproduce and extend [10]. These limitations motivate the central research problem of this thesis: How can we design, implement and evaluate an automated, calibration aware TEM analysis pipeline that accurately segments etioplast ultrastructure, produces reliable morphometric measurements, and can be delivered as a practical web application for routine use in plastid biology?

 

## 1.4 Research Question

- How accurately can YOLO based instance segmentation models detect and segment etioplasts and their internal structures (PLBs, PTs, plastoglobules and starch) in TEM images when they are trained on expert validated annotations?
- To what extent do morphometric parameters derived from automated segmentations, such as etioplast area, PLB area, prothylakoid number and total length, and plastoglobule number and diameter, agree with measurements obtained manually by an experienced expert?
- How do preprocessing and data augmentation choices influence segmentation accuracy and downstream parameter estimates across different image qualities and magnifications?
- Can the trained model, measurement pipeline and calibration logic be integrated into a web based application that offers plant biologists an efficient, reproducible and easy to use tool for quantitative etioplast analysis?

## 1.5 Research Objective

The main objective of this thesis is to develop and evaluate an automated TEM based framework for quantitative analysis of etioplast ultrastructure. The specific objectives are:

- To curate a dataset of TEM images of etioplasts, including expert annotated masks for etioplast envelopes, PLBs, PTs, plastoglobules and starch, together with reliable pixel size calibration.
- To design and train multiple YOLO based instance segmentation models (YOLOv5-seg, YOLOv8-seg and YOLOv12-seg) on this dataset, and to select a final model based on validation performance.
- To implement a measurement module that converts segmentation masks into calibrated morphometric features for each etioplast, including areas, perimeters, counts, total lengths, shape descriptors and basic quality control flags.
- To define and apply a set of quantitative evaluation metrics, including Dice, IoU, precision, recall, F1 score and parameter error measures (MAE, RMSE, MAPE and Bland Altman analysis), in order to compare automated outputs with expert derived measurements.
- To deploy the best performing model and measurement pipeline as a web based application that allows users to upload TEM images, run inference, visualize segmentation overlays, download measurement tables and view short textual summaries generated by a post hoc generative AI component.

.

## 1.6 Contribution

- An end to end, TEM-specific analysis pipeline for etioplast ultrastructure that uses YOLO based instance segmentation to detect etioplast envelopes, prolamellar bodies (PLBs), prothylakoids (PTs), plastoglobules and starch grains directly from TEM micrographs.

 

- A calibration aware measurement framework that converts segmentation masks into etioplast specific morphometric features (areas, lengths, counts, shape descriptors) in physical units, making measurements comparable across images, sessions and experiments.
- A quality control module and evaluation strategy that highlight the strengths and limitations of the approach, including practical conditions under which automated measurements are reliable and situations where human review remains necessary.
- A web based implementation, “Etioplast Detector AI”, that packages the trained model and measurement pipeline into a user-friendly interface, allowing plant biologists to upload images, inspect segmentation overlays and download quantitative results without writing code.
- A reproducible, well documented workflow with clearly organized data, configuration files, figures and tables that can serve as a starting point for future projects in quantitative plant ultrastructure analysis and, in future extensions, nanoparticle uptake studies.

# Chapter 2

# Literature review

## 2.1 Introduction

Plastid biology, transmission electron microscopy (TEM) and automated image analysis together frame this work. Etioplasts form in tissues grown without light and rapidly differentiate into chloroplasts after illumination [5]. Their ultrastructure prolamellar body (PLB), prothylakoid membranes (PTs), lipid rich plastoglobules and occasional starch grains reflects plastid development, stress responses and genetic changes, but is hard to quantify consistently across many samples [5]. TEM is the main technique for viewing these nanometer scale structures [6]. Standard preparation and high voltage imaging yield detailed views of membranes and plastoglobules, yet most quantitative studies still depend on manual or semi-automated tracing in ImageJ or similar tools [11]. This is slow, subjective and difficult to reproduce, limiting large scale comparative analyses. To reduce this burden, automated tools have been proposed for chloroplast ultrastructure, using thresholding, edge detection, Fourier analysis and CNN based segmentation, sometimes combined with expert correction [10]. These methods, however, focus on mature chloroplasts, and there is still no widely used software for automated etioplast segmentation and morphometrics [21]. Deep learning, including U Net style networks and YOLO based instance segmentation, has already improved organelle and membrane segmentation in electron microscopy [1], but successful application to etioplasts requires careful preprocessing, realistic augmentation and sufficient annotated data. Reliable morphometrics also depend on explicit pixel size calibration and transparent, version-controlled data and code. Together, these gaps in automation, calibration handling and reproducibility motivate the etioplast specific pipeline developed in this thesis.

 

## 2.2 Literature Review

[1] Ronneberger, O., Fischer, P., and Brox, T. propose U-Net, an encoder–decoder convolutional network with skip connections tailored for fast and precise biomedical image segmentation from limited annotated data. The architecture combines a contracting path for contextual encoding with a symmetric expanding path for accurate localization and heavy data augmentation, and it has become a standard backbone for segmenting cellular and subcellular structures in microscopy, including EM images relevant to plastid morphology.

[2] Otsu, N. introduces a nonparametric, unsupervised global thresholding method that selects the optimal gray-level threshold by maximizing between-class variance in the image histogram. This simple yet powerful criterion remains a widely used baseline for image binarization and mask generation, especially in segmentation pipelines where no prior label information is available.

[3] Dabov, K., Foi, A., Katkovnik, V., and Egiazarian, K. present the BM3D algorithm, a transform-domain denoising method that groups similar image patches into 3D blocks and applies collaborative filtering to exploit sparse representations. Their approach achieves state-of-the-art noise suppression while preserving fine structural details, making it particularly suitable as a preprocessing step for high-resolution EM images of plastids and nanoparticle-containing tissues.

[4] Bland, J. M., and Altman, D. G. develop a statistical framework for assessing agreement between two measurement methods based on mean bias and limits of agreement. The Bland–Altman plot has become a standard tool for method comparison, providing a more informative view of measurement concordance than correlation alone and directly supporting validation of automated morphometric pipelines against expert manual tracing.

[5] Solymosi, K., and Bóka, J. review etioplasts as key intermediates in plastid differentiation and chloroplast biogenesis, summarizing their inner-membrane architecture, pigment composition, and developmental dynamics in etiolated tissues. They highlight both the strengths and limitations of using etioplasts as laboratory models of chloroplast formation, laying a biological foundation for quantitative analyses of prolamellar bodies (PLBs) and prothylakoids.

[6] Floris, D. et al. use electron cryo-tomography to map the molecular landscape of etioplast inner membranes in higher plants, revealing distinct protein distributions in PLBs and prothylakoids. Their reconstructions show ATP synthase enrichment in prothylakoids, ribosomes localized to the tubular lattice, and LPOR forming helical arrays on PLB membranes, providing mechanistic insight into how protein organization underpins etioplast membrane geometry.

[7] Liang, Z. et al. apply electron tomography to follow PLB architecture and its transformation during de-etiolation, reconstructing how the paracrystalline

 

cubic lattice remodels into thylakoid membranes under light. By capturing intermediate states and topological transitions, the study links nanoscale membrane rearrangements in PLBs to the emergence of functional grana and stroma thylakoids during chloroplast biogenesis.

[8] Bykowski, M. et al. investigate the spatial nano-morphology of PLBs in etiolated cotyledons, combining high-resolution EM with quantitative image analysis to characterize lattice symmetry, periodicity, and local curvature. Their work demonstrates how subtle variations in PLB nano-architecture correlate with developmental state and environmental conditions, and it provides concrete measurement strategies for extracting morphometric descriptors from 2D and 3D data.

[9] Selstam, E., and Sandelius, G. study the structural organization of PLBs isolated from dark-grown leaves, integrating ultrastructural observations with biochemical characterization of lipids and POR complexes. They propose how pigment–protein aggregates and specific lipid compositions contribute to the formation and stability of the paracrystalline tubular network, offering a biophysical context for interpreting PLB morphology in situ and in vitro.

[10] Bukat, A. et al. Presenting GRANA, an AI-based tool that combines three neural networks to provide a 1-click workflow for 2D TEM images of chloroplast thylakoids: a YOLOv8-based detector for grana masks, a ResNet18-based orientation estimator, and an attention-enhanced CNN for stacking repeat distance. Key grana nanomorphology features (area, perimeter, height, diameter, SRD, thylakoid number, and GSI) are automatically extracted by the software, which also provides standardized, repeatable measurements through fully automated and hybrid (AI + expert) modes considerably more quickly than with traditional manual ImageJ analysis.

[12] Wang, X. et al. review nanoparticle uptake, transport, and physiological effects in plants, summarizing key entry routes (e.g., root and foliar), translocation pathways (apoplastic vs. symplastic), and downstream impacts on growth and stress responses. By emphasizing how particle size, surface chemistry, and plant species jointly determine uptake and toxicity, the paper motivates precise, quantitative localization of nanoparticles within subcellular compartments, including plastids.

[14] Djanaguiraman, M. et al. synthesize current knowledge on nanoparticle uptake, translocation, toxicity, and broader impacts in plants, with an emphasis on major crops and stress physiology. Their review balances beneficial uses of nano-enabled inputs with potential risks, arguing for carefully designed experiments that integrate physiological readouts with ultrastructural evidence from TEM to pinpoint nanoparticle localization and damage.

[15] Raliya, R., Tarafdar, J. C., and Biswas, P. address the quantitative side of nanoparticle uptake in plants, using controlled experiments and analytical

 

techniques to measure mass fluxes and spatial distribution. They propose frameworks that relate nanoparticle dose, size, and chemistry to uptake efficiency and internal partitioning, providing a conceptual basis for linking TEM-based particle counts to whole-tissue or whole-plant exposure metrics.

[17] Kempen, P. J. et al. present a scanning transmission electron microscopy (STEM) workflow optimized for detecting and analyzing nanoparticles across large tissue volumes. Their approach combines high-angle annular dark-field imaging with systematic tiling and automated analysis to find rare particles, offering a scalable template for nanoparticle detection that can be adapted to plant sections and etioplast-containing regions.

[21] Li et al. (2024), Sharma et al. (2024), Khruschev et al. (2022), Nomura et al. (2023), Armarego-Marriott et al. (2019), Pipitone et al. (2021), and Sajib et al. (2023), as cited in the slide deck, collectively extend this literature by providing recent advances in etioplast and thylakoid ultrastructure, de-etiolation dynamics, and nanoparticle–plastid interactions, as well as domain-specific image-analysis tools. Although their individual scopes differ, together they reinforce the need for standardized, automated TEM pipelines that can bridge high-resolution morphology, nanoparticle localization, and functional plant responses within a single quantitative framework.

## 2.3 Research Gap

- No etioplast-focused analysis tools. There is no commonly used software that automatically segments PLB/PT structures in etioplasts and extracts detailed, plastid-specific morphometric features.

- Lack of dual-pipeline, consensus-based frameworks. TEM image analysis rarely combines classical image processing and deep learning in a single framework that explicitly measures and uses agreement between the two.

- Uncertainty and expert agreement are not routinely quantified. Calibration, segmentation uncertainty, and systematic comparison with expert measurements are often glossed over or only partially reported.

# Chapter 3

## Methodology

### 3.1 Introduction

The proposed system has two main stages: an offline model development stage and an online deployment stage, as outlined in the methodology diagram (Fig.1). In the offline stage, raw TEM micrographs are first annotated by hand and checked by a domain expert. The curated dataset is then split into training, validation, and test subsets and expanded through data augmentation. On this processed dataset, YOLOv5-seg, YOLOv8-seg, and YOLOv12-seg models are trained for segmentation. The best-performing checkpoint, selected based on validation metrics, is saved as a .pt file and further evaluated on the held-out test set in the online stage, a client can submit new TEM images through an API. The server loads the selected YOLO model, applies the necessary preprocessing and calibration steps, and then runs inference. Post-processing modules convert the segmentation outputs into quantitative morphometric measurements and quality control flags. Finally, a generative-AI component uses only these numerical results to produce a short textual summary. The client receives both the structured outputs (e.g., JSON or CSV) and the accompanying narrative description.

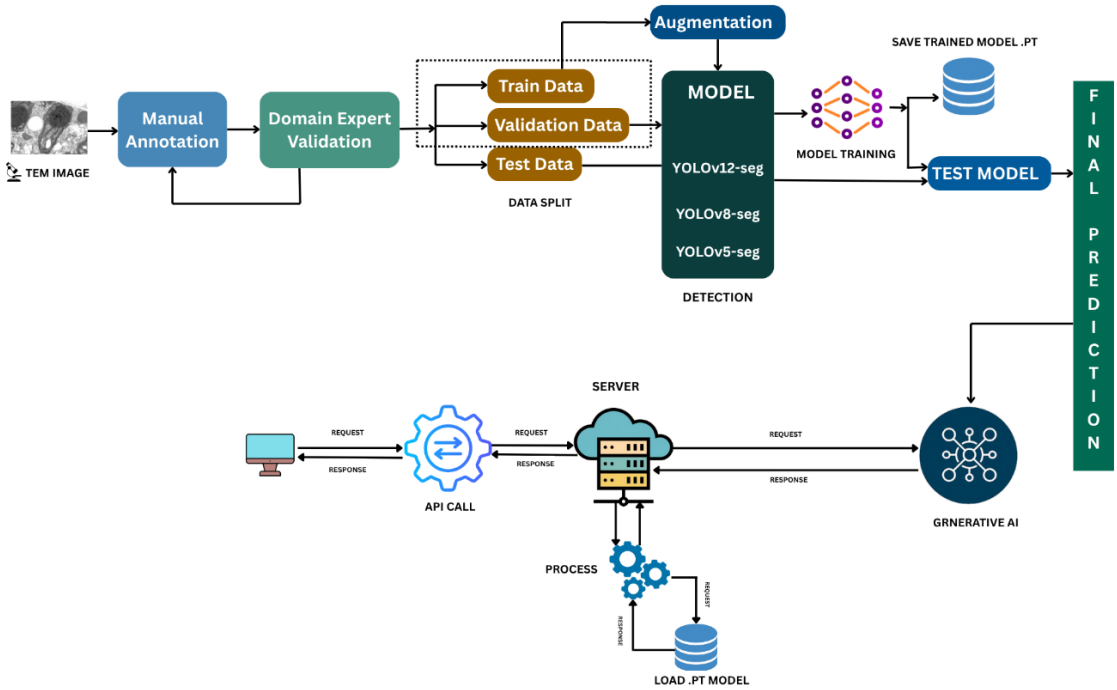


Figure 3.1.1: Methodology

## 3.2 Data Collection and Curation

The dataset used in this thesis consists of 230 TEM micrographs of etioplast-containing tissues, provided by a collaborating research group at a CNRS laboratory in France. All images were taken from Arabidopsis thaliana (ecotype Col-0) seedlings grown in darkness for 3–4 days. The focus was on non-green cotyledons and the apical hook/upper hypocotyl region, as these tissues are known to contain many etioplasts. Sample preparation and TEM imaging were carried out entirely by the CNRS team; in this project, I work only with the resulting digital micrographs and their associated metadata. The images were supplied as 16-bit TIFF files with embedded scale bars, along with metadata describing key acquisition settings (such as accelerating voltage and magnification) and tissue type. After receiving the data, I organized it into a reproducible folder structure that separates raw images, annotations, and processed outputs. Each specimen was given an anonymized identifier so that images from the same biological source could be tracked and grouped later during analysis. I also performed a light curation step to remove any clearly corrupted or unusable images so that only quality-checked micrographs entered the automated segmentation and measurement pipeline.

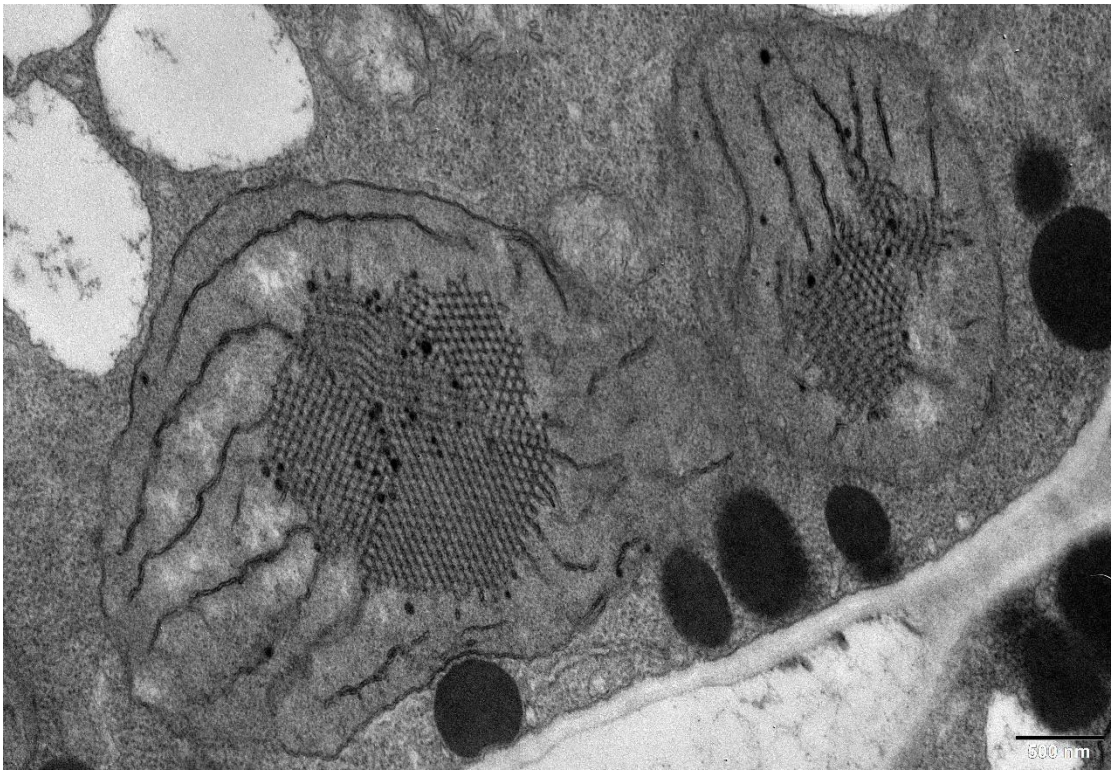


Figure 3.1.2: TEM image of an Etioplast

 

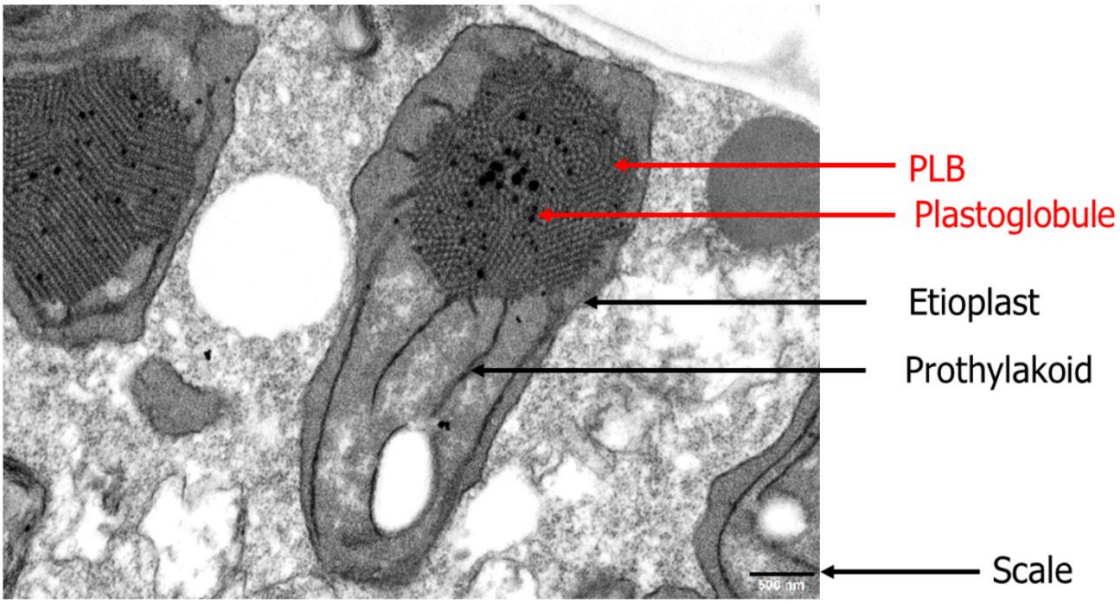


Figure 3.1.3: Structure of the Etioplast

## 3.3 Manual Annotation and Domain Expert Validation

Manual annotations were created using the open-source labeling tool **CVAT**. For each image, I used polygon shapes to carefully outline the main structures of interest:

- Etioplast envelope
- PLB region
- PT membranes
- Starch grains

For **plastoglobules**, which are typically small and rounded, I used **ellipse shapes** so that the annotations would better reflect their actual geometry. Once the first round of annotations was complete, every image was reviewed by a plastid-biology expert. The expert corrected inaccurate segmentations, added any structures I had missed, and removed images that were too unclear to label with confidence. We repeated this review-and-correction cycle until we were both satisfied with the quality of the masks. The final, expert-approved annotations form the ground truth used for training the models and for all quantitative evaluations in this thesis

### 3.3.1 Manual Annotation:

 

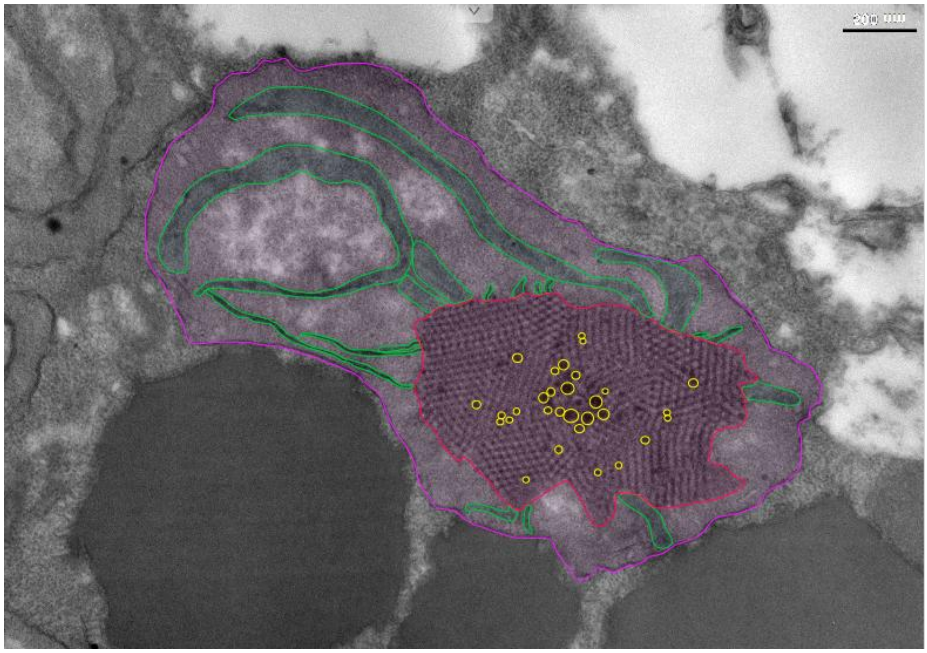

Figure 3.3.1: Manual Annotation with CVAT

### 3.3.2 Domain Expert Validation

An expert plastid specialist reviews all preliminary annotations in this step. The specialist thoroughly reviews every annotated structure, points out mistakes, omitted areas, and discrepancies, and offers written suggestions for enhancement. I update the annotations and create a new, corrected set of masks based on this feedback. The final ground truth for all ensuing analyses and model evaluations in this thesis is then these expert-approved masks.

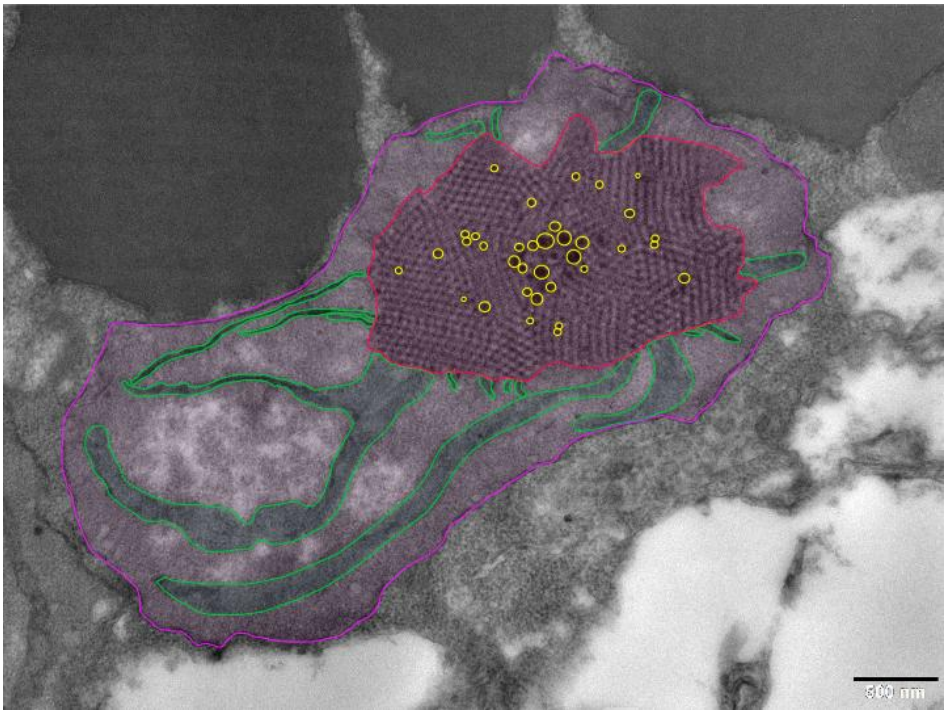

Figure 3.3.2: After Expert Validation

### 3.4 Dataset Splitting and Augmentation

Validated images were split into training, validation, and test sets using a stratified strategy based on specimen and grid identifiers to avoid data leakage. In all experiments, 80% of the images were used for training, 10% for validation, and 10% for testing. To further reduce information leakage, images coming from the same section or grid square were always kept together in a single subset and were never spread across different splits. For the training set, I applied label-preserving data augmentations such as horizontal and vertical flips, 90° rotations, small isotropic scaling, elastic deformations, brightness and contrast adjustments, and mild Gaussian noise or blur. These transformations were chosen to reflect realistic variability in TEM imaging while still preserving key biological structures, including etioplast boundaries, PLB lattices, and nanoparticle shapes. The validation and test sets were processed only with the standard preprocessing pipeline and did not receive any geometric or intensity augmentations.

## 3.5 Preprocessing

The preprocessing module behaves the same way in both the offline and online stages. For each image, it applies a series of steps:

- Denoising: High-frequency noise is reduced using a BM3D-like or non-local means filter, with parameters chosen to smooth the background while preserving sharp membrane boundaries [3].

- Contrast normalization: Image intensities are normalized using percentile-based clipping followed by linear rescaling so that the full dynamic range is effectively used.

- Background correction: Slow intensity variations caused by uneven staining or illumination are removed using large-kernel smoothing or morphological opening.

- Scale calibration: The pixel size is obtained either directly from stored metadata or, when necessary, by interactively measuring the visible scale bar. Both the calibration factor and its estimated uncertainty are recorded for each image.

 

### 3.6 YOLO-based Organellar Segmentation

Three YOLO-based instance segmentation models were explored in this work: **YOLOv5-seg**, **YOLOv8-seg**, and **YOLOv12-seg**. Each model was set up with multiple output classes to separately detect etioplasts, PLBs, PTs, plastoglobules, and starch. Training was carried out on the augmented training set using the standard YOLO loss, which combines bounding-box regression, classification, and mask loss, and was optimized with the AdamW optimizer. Key hyperparameters such as learning rate, batch size, and number of epochs were tuned using the validation set. To reduce overfitting, I applied early stopping based on validation loss and Dice score. For each YOLO variant, the checkpoint that achieved the best validation performance was saved as a .pt file and used for further evaluation.

#### 3.6.1 YOLOv5-seg

YOLOv5-seg represents a mature, anchor-based family of models that balances accuracy and computational cost. It uses a convolutional backbone for feature extraction, a feature pyramid/neck for multi-scale features, and a detection head that predicts bounding boxes, class probabilities, objectness scores, and segmentation masks.

For each grid cell g and anchor a, YOLOv5-seg predicts a vector

$$\boldsymbol{y\_hat\_}(\boldsymbol{g}, \boldsymbol{a}) = (\boldsymbol{p\_obj}, \boldsymbol{p\_cls}[\mathbf{1}..\boldsymbol{C}], \boldsymbol{x}, \boldsymbol{y}, \boldsymbol{w}, \boldsymbol{h}, \boldsymbol{m})$$

where:

- p_obj is the objectness score,
- p_cls[1..C] is the C-dimensional class probability vector,
- (x, y, w, h) are the box coordinates (center x, center y, width, height),
- m is a low-resolution mask prototype or mask coefficients.

The bounding box loss is typically a variant of IoU-based loss such as CIoU or GIoU. In simplified form, we can write

$$\boldsymbol{L\_box} = \mathbf{1} - \boldsymbol{IoU}(\boldsymbol{b\_pred}, \boldsymbol{b\_gt})$$

where b_pred and b_gt are the predicted and ground-truth boxes.

The objectness and classification losses use binary cross-entropy (BCE):

$$\boldsymbol{L\_obj} = \boldsymbol{BCE}(\boldsymbol{p\_obj}, \boldsymbol{p\_obj}*)$$
$$\boldsymbol{L\_cls} = \boldsymbol{BCE}(\boldsymbol{p\_cls}, \boldsymbol{p\_cls}*)$$

where the asterisk (*) denotes ground-truth values (1 for the correct class/object, 0 otherwise).

 

For the segmentation mask, a combination of BCE and Dice loss is commonly used:

$$L\_mask = BCE(m, m*) + L\_Dice(m, m*)$$

where the Dice loss term measures overlap between predicted and ground-truth masks:

$$L\_Dice(m, m*) = 1 - (2 * sum(m * m*)) / (sum(m) + sum(m*) + \varepsilon)$$

Here sum(·) denotes summation over all pixels and ε is a small constant to avoid division by zero.

Because YOLOv5-seg is comparatively lightweight and uses anchors, it converges stably on relatively small datasets and provides fast inference, which is advantageous for batch processing TEM images of etioplast ultrastructure.

### 3.6.2 YOLOv8-seg

YOLOv8-seg is a more recent, anchor-free evolution of the YOLO family. Instead of predefined anchor boxes, it directly predicts key quantities for each candidate point (for example, center location and distances to box sides), which simplifies training and can improve generalization across scale and aspect ratio.

For each candidate point i, YOLOv8-seg predicts:

$$y\_hat\_i = (p\_obj, p\_cls[1..C], d\_left, d\_top, d\_right, d\_bottom, m)$$

where:

- (d_left, d_top, d_right, d_bottom) encode the bounding box by distances from the point to each side of the box,
- other symbols are as defined above.

The predicted distances define a box b_pred^(i). The bounding-box loss again uses an IoU-style term, but often with a more refined formulation (for example, distribution-aware distance regression). Conceptually:

$$L\_box = 1 - IoU(b\_pred\hat{}(i), b\_gt\hat{}(i))$$

The classification and objectness branches use BCE or focal loss. A generic focal-style classification loss can be written as:

$$L\_cls = -\alpha * (1 - p\_cls\_t)\hat{}\gamma * log(p\_cls\_t)$$

where:

 

- p_cls_t is the predicted probability for the true class,
- α is a balancing factor,
- γ is the focusing parameter that down-weights easy examples.

The segmentation loss keeps the same structure as before:

$$\boldsymbol{L\_mask} = \boldsymbol{BCE}(\boldsymbol{m}, \boldsymbol{m}*) + \boldsymbol{L\_Dice}(\boldsymbol{m}, \boldsymbol{m}*)$$

By decoupling classification and regression heads and by avoiding anchors, YOLOv8-seg can better adapt to the diverse sizes and shapes of PLBs, PTs, and plastoglobules. This is particularly helpful for thin, elongated membranes and small, nearly circular droplets in TEM micrographs.

### 3.6.3 YOLOv12-seg

YOLOv12-seg is considered in this thesis as a representative of newer-generation YOLO models that integrate more advanced backbone designs, feature fusion strategies, and training heuristics. The exact implementation can vary, but the underlying idea remains a single-stage, multi-task network for object detection and instance segmentation.

At each prediction location j, YOLOv12-seg outputs:

$$\boldsymbol{y\_hat\_j} = (\boldsymbol{p\_obj}, \boldsymbol{p\_cls}[\mathbf{1}..\boldsymbol{C}], \boldsymbol{b\_j}, \boldsymbol{m\_j})$$

where:

- b_j represents box parameters (which may be parameterized by center/size or distance-to-sides, depending on the variant),
- m_j is the corresponding mask prediction.

The total loss follows the same multi-task structure:

$$\boldsymbol{L} = \boldsymbol{\lambda\_box} * \boldsymbol{L\_box}(\boldsymbol{b\_j}, \boldsymbol{b\_j}*)$$

- $\boldsymbol{\lambda\_obj} * \boldsymbol{L\_obj}(\boldsymbol{p\_obj}, \boldsymbol{p\_obj}*)$
- $\boldsymbol{\lambda\_cls} * \boldsymbol{L\_cls}(\boldsymbol{p\_cls}, \boldsymbol{p\_cls}*)$
- $\boldsymbol{\lambda\_mask} * \boldsymbol{L\_mask}(\boldsymbol{m\_j}, \boldsymbol{m\_j}*)$

In newer YOLO-style models, L_box may use more advanced IoU variants (for example, CIoU/EIoU), L_cls may use improved focal or distribution-based losses, and L_mask often combines pixel-wise BCE with region-level overlap measures (Dice or IoU loss). Conceptually, we can summarize:

$$\boldsymbol{L\_box} \approx \mathbf{1} - \boldsymbol{IoU\_variant}(\boldsymbol{b\_j}, \boldsymbol{b\_j}*)$$
$$\boldsymbol{L\_obj} \approx \boldsymbol{BCE}(\boldsymbol{p\_obj}, \boldsymbol{p\_obj}*)$$
$$\boldsymbol{L\_cls} \approx \boldsymbol{focal - BCE\ on\ class\ scores}$$

 

$$L\_mask \approx BCE(m\_j, m\_j*) + Dice - loss(m\_j, m\_j*)$$

## 3.7 Measurement and Feature Extraction

The Measurement module converts the predicted instance masks into quantitative morphometric features for each detected etioplast. Building on the theoretical concepts introduced in Chapter 3, it first operates in pixel space and then converts all quantities into calibrated physical units. For every etioplast in an image, the module computes:

- etioplast area and perimeter;
- PLB area and relative PLB occupancy (PLB area / etioplast area);
- PT count and total PT length (from skeletonized masks);
- plastoglobule count and individual equivalent diameters, with mean and standard deviation;
- optional starch area per etioplast.

All measurements are stored in physical units using the image-specific calibration **s**. Basic shape descriptors such as circularity and aspect ratio are computed for etioplasts and plastoglobules to capture morphological changes.
To make these operations explicit, let $\mathbf{X_e}$, **X_PLB**, **X_PT**, **X_PG**, and **X_st** denote the binary masks for the etioplast envelope, prolamellar body, prothylakoids, plastoglobules, and starch, respectively.
The pixel size **s** (in nm/px) is obtained from the scale bar or metadata as:

$$s = \frac{scale_{nm}}{scale_{px}}$$

where scale_nm is the physical length (nm) represented by the scale bar and scale_px is the corresponding length in pixels.

### 3.7.1 Areas, Perimeters, and Shape Descriptors

For each etioplast instance **k**, the model returns a connected component $\mathbf{X_e(k)}$. Its area in pixels is $|X_e(k)|$. The corresponding physical area in nm² is:

$$A_e(k) = |X_e(k)| \cdot s^2$$

To express the same area in μm²:

 

$$A_{e}\_\mu m^2(k) = A_{e}(k) / 10^6$$

The perimeter $\mathbf{P_e(k)}$ is obtained from the contour of $\mathbf{X_e(k)}$ (in nm after calibration). Circularity **C(k)** is defined as:

$$C(k) = 4\pi \cdot A_{e}(k) / [P_{e}(k)]^2$$

Aspect ratio is computed as:

$$aspect\_ratio(k) = major\_axis(k) / minor\_axis(k)$$

where major_axis(k) and minor_axis(k) are the lengths of the major and minor axes of the best-fit ellipse to $\mathbf{X_e(k)}$.

The same operations are applied to the PLB mask **X_PLB(k)**, giving the PLB area **A_PLB(k)** and the relative PLB occupancy:

$$R\_PLB(k) = A\_PLB(k) / A_{e}(k)$$

If a starch mask **X_st(k)** is present, its area **A_st(k)** is computed analogously:
$A\_st(k) = |X\_st(k)| \cdot s^2$
(and can also be converted to μm² by dividing by $10^6$, if needed).

### 3.7.2 Prothylakoid Morphometrics

Prothylakoids are represented by the mask **X_PT(k)**. To obtain length-based descriptors:
The mask is skeletonized with a topology-preserving thinning algorithm, resulting in a one-pixel-wide centerline. The skeleton is decomposed into segments **p = 1, …, N_PT(k)** between branch/junction points. For each segment, the geodesic length in pixels **L_p** is measured and converted to nanometers as:

$$L\_p\_nm = L\_p \cdot s$$

For etioplast **k**, the module reports:
PT count:

$$N\_PT(k)\ (number\ of\ skeleton\ segments)$$

Total PT length (in nm):

$$L\_PT(k) = \Sigma\ (from\ p = 1\ to\ N\_PT(k))\ L\_p\_nm$$

Optional statistics such as mean segment length and its standard deviation can also be derived:

 

$$mean\_L\_PT(k) = [1 / N\_PT(k)] \cdot \Sigma\, L\_p\_nm$$

$$std\_L\_PT(k)\ (standard\ deviation\ of\ the\ L\_p\_nm\ values)$$

### 3.7.3 Plastoglobule Morphometrics

Each detected plastoglobule instance belonging to etioplast **k** is a connected component **X_PG(k, j)**. Treating plastoglobules as approximately circular objects, their equivalent area and diameter are defined as follows.
First, compute area in nm²:

$$A\_PG(k,j) = |X\_PG(k,j)| \cdot s^2$$

Then compute the equivalent diameter (assuming a circle of area A_PG):

$$d\_PG(k,j) = 2 \cdot \sqrt{(A\_PG(k,j) / \pi)}$$

The module then aggregates, per etioplast **k**:
plastoglobule count:

$$N\_PG(k) = number\ of\ j\ for\ which\ X\_PG(k,j)\ exists$$

mean equivalent diameter:

$$đ\_PG(k) = [1 / N\_PG(k)] \cdot \Sigma\, d\_PG(k,j)$$

standard deviation of the equivalent diameters:

$$std\_d\_PG(k) = \sqrt{\{ [1 / (N\_PG(k) - 1)] \cdot \Sigma\, [d\_PG(k,j) - đ\_PG(k)]^2 \}}$$

### 3.7.4 Etioplast Feature Vector and Storage

For each etioplast instance **k**, the Measurement module outputs a standardized feature vector:

***f(k) = [***
***Ae(k),***
***APLB(k),***
***RPLB(k),***
***NPT(k),***
***LPT(k),***
***NPG(k),***
***d_bar_PG(k),***
***shape_descriptors(k),***
***QC_flags(k),***

 

...
*J*

## 3.8 Quality Control

To avoid reporting unreliable results, a Quality Control (QC) module evaluates both the input images and the model predictions. At the image level, the system checks for issues such as very low global contrast, excessive noise, saturation, or a missing/ambiguous scale bar. At the prediction level, it looks for warning signs like very low mean confidence scores, biologically implausible sizes (for example, etioplast areas falling below a user-defined minimum), or inconsistent patterns (such as zero PT length in images that clearly contain structured membranes). Images that fail one or more QC checks are flagged. Their measurements are either excluded from automatic aggregation or explicitly marked for manual review. All QC flags are included in the structured outputs so that users can easily identify and handle questionable cases.

## 3.9 Generative AI Interpreter

The Generative AI module is implemented as a lightweight language model or a simple templated reporting system that receives only the finalized numeric outputs and QC flags from the measurement and quality-control modules. It does **not** access the raw images or rerun any inference. Instead, its role is to turn structured numeric records into short, human-readable summaries. Given a per-image record, the interpreter can generate text of the following form:

"One etioplast was detected (area 4.8 μm²). The prolamellar body occupied 1.9 μm² (40% of the plastid area), with 27 prothylakoids totaling 12.3 μm in length. Sixteen plastoglobules were identified, with a mean diameter of 47.2 nm. No starch grains were detected. QC: measurements passed all internal checks."

Here, the specific numbers are inserted directly from the computed measurements and associated QC flags. The interpreter is explicitly restricted from modifying these values or performing any additional analysis; it simply reformats and contextualizes them. This design keeps the generative component transparent and ensures that all reported statements remain traceable back to the underlying quantitative results.

## 3.10 Algorithm 1: Offline Training Pipeline

Algorithm 1: Offline YOLO-Seg Training for Etioplast Ultrastructure

 

Input: Raw TEM images, metadata, expert annotations
Output: Trained YOLO-Seg checkpoint best_model.pt

1: Collect raw TEM images and associated metadata from [Dataset Placeholder].
2: For each image do
3: Apply preprocessing (denoising, intensity normalization, scale calibration).
4: Obtain or refine etioplast / PLB / NP annotations with expert validation.
5: end for
6: Split the dataset into train/validation/test subsets (80% / 10% / 10%)
7: Ensure that images from the same specimen or grid square appear in only one subset.
8: Apply label-preserving data augmentations to the training set (flips, rotations, scaling, elastic deformation, brightness/contrast jitter, mild noise/blur).
9: For each YOLO-Seg variant m ∈ {v5-seg, v8-seg, v12-seg} do
10: Initialize model m with pretrained weights.
11: while training has not converged do
12: Sample a mini-batch from the training set.
13: Compute YOLO segmentation loss (bounding box + class + mask terms).
14: Update model weights using the AdamW optimizer.
15: Periodically evaluate m on the validation set (Dice, IoU, F1).
16: Apply learning-rate scheduling and early stopping criteria.
17: end while
18: Save the best-performing checkpoint for model m as model_m_best.pt.
19: end for
20: Evaluate all model_m_best.pt checkpoints on the held-out test set.
21: Select best_model.pt based on accuracy–speed trade-off.
22: Return best_model.pt.

### 3.11 Algorithm 2: Online Inference and Deployment

Algorithm 2: Online Inference and Measurement via API

Input: New TEM image submitted by a client
Output: Structured numeric results + textual summary

1: Client sends an HTTP request containing the TEM image file.
2: Server validates the request (file type, size) and logs basic metadata (timestamp, client ID, filename, optional specimen ID).
3: Preprocessor module denoises the image, normalizes intensities, and applies scale calibration using metadata or a detected scale bar.
4: Load best_model.pt into memory if it is not already loaded.

 

5: Run YOLO-Seg inference on the preprocessed image to obtain
segmentation masks, bounding boxes, class labels, and confidence scores.
6: Measurement module computes per-etioplast morphometrics
(areas, perimeters, circularity, aspect ratios, PLB/PT fractions,
nanoparticle counts and size statistics).
7: Quality Controller evaluates image and prediction quality
(e.g., low-contrast flags, suspicious calibration, out-of-distribution patterns).
8: Master Aggregator assembles all outputs into a structured record
(metrics, QC flags, intermediate IDs and masks).
9: Pass the aggregated record to the Gen-AI interpreter.
10: Gen-AI module generates a concise textual summary explaining the key
findings (e.g., etioplast morphology, PLB organization, NP uptake).
11: Server returns a JSON response to the client containing
(i) numeric metrics and QC flags, and
(ii) the generated textual summary.

### 3.12 Algorithm 3: Generative AI Interpretation

Algorithm 3: Gen-AI Textual Summary Generator

Input: Aggregated record R (masks, metrics, QC flags)
Output: Human-readable summary S

1: From R, extract key quantitative and qualitative values, including
etioplast and PLB/PT areas, perimeters, aspect ratios, NP counts,
NP size statistics, and all QC flags.
2: Construct a structured prompt P that:
(a) lists all extracted numeric values explicitly,
(b) clearly states that these values must not be altered,
(c) specifies the desired output style (concise, formal, scientific tone),
(d) indicates the intended audience (e.g., plant biologist, microscopist).
3: Provide P as input to the language model (Gen-AI module).
4: Receive the candidate textual summary S generated by the model.
5: Optionally perform a post-check on S to verify:
(a) strict consistency between the text and the numeric values in R,
(b) absence of unsupported claims, hallucinated measurements, or
forbidden wording (e.g., overstated causality).
6: If required, revise P or apply lightweight rule-based edits and
regenerate S.
7: Return the final summary S.

 

## 3.12 Data Management, Ethics, and Safety

All image data are stored in a non-lossy format (TIFF), with full metadata retained, including acquisition parameters and calibration information. The directory structure is organized by specimen and imaging session, and file names use only specimen codes and imaging parameters, avoiding any personal or sensitive identifiers. All preprocessing, training, and evaluation scripts are kept under version control, along with their configuration files and logs, so that the full analysis can be reproduced step by step. Plant material was handled in line with the ethical and biosafety guidelines of the collaborating CNRS and university laboratories. Sample preparation followed standard TEM protocols, using common fixatives and stains (such as glutaraldehyde, osmium tetroxide, and uranyl acetate). These chemicals were handled exclusively with appropriate personal protective equipment and within certified fume hoods. Chemical waste and contaminated consumables were disposed of according to institutional hazardous-waste procedures. No human or animal subjects were involved in this study. Issues of bias and robustness such as dataset balance, stratified splitting, and augmentation strategies are discussed in more detail in the following chapter.

# Chapter 4

# Result and Discussion

## 4.1 Introduction

This chapter presents the experimental performance of the proposed TEM based etioplast analysis pipeline. The results are organized around three main aspects: (i) the segmentation quality of the YOLO models for etioplast envelopes, prolamellar bodies (PLBs), prothylakoids (PTs), plastoglobules and starch grains; (ii) the behavior of the derived morphometric measurements compared to expert judgement; and (iii) practical considerations, including the impact of preprocessing, data augmentation and web based deployment. Two lightweight instance segmentation models, YOLO11n-seg and YOLOv8n-seg, were trained on the same curated dataset and evaluated on a held out validation set. Based on these results, YOLO11n-seg was selected as the final model and integrated into the Etioplast Detector AI web application. The following sections describe the segmentation performance, parameter accuracy, ablation experiments and comparison with manual workflows, and then summaries feedback from an independent plastid expert.

 

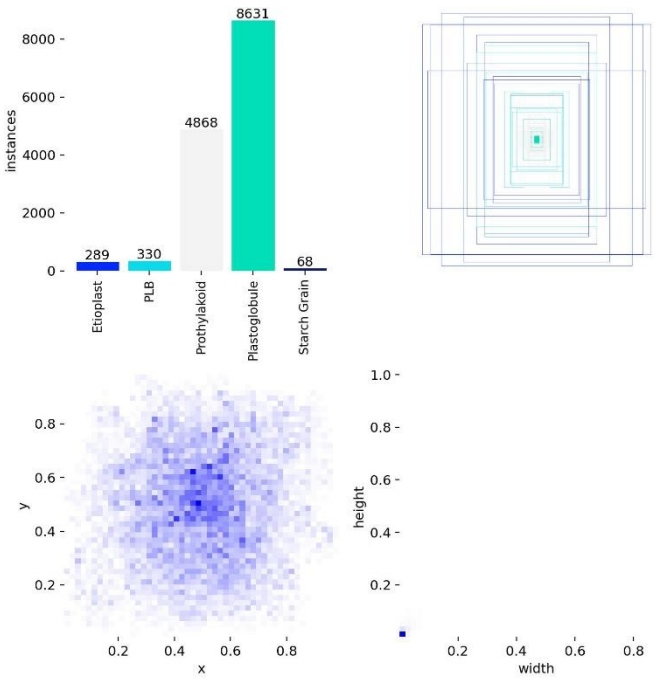


Figure 4.1.1: Dataset summary

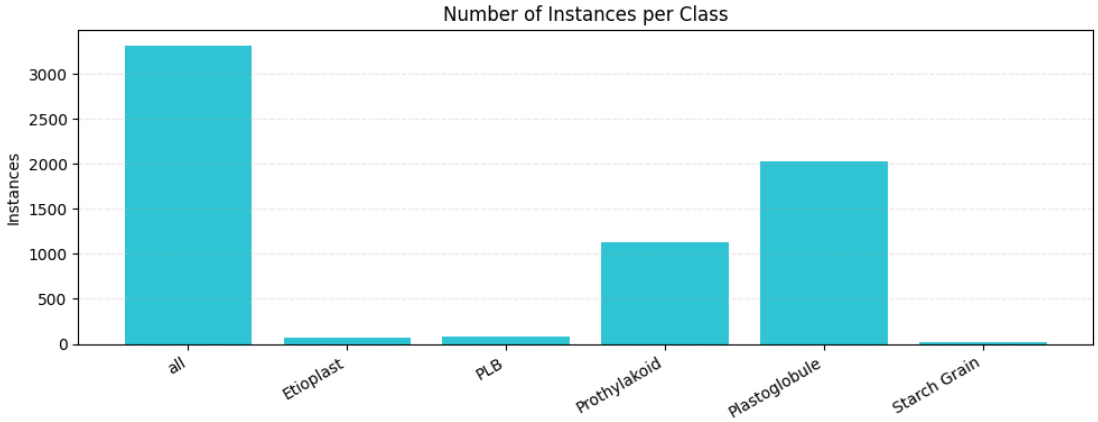


Figure 4.1.2 Number of instances per Class

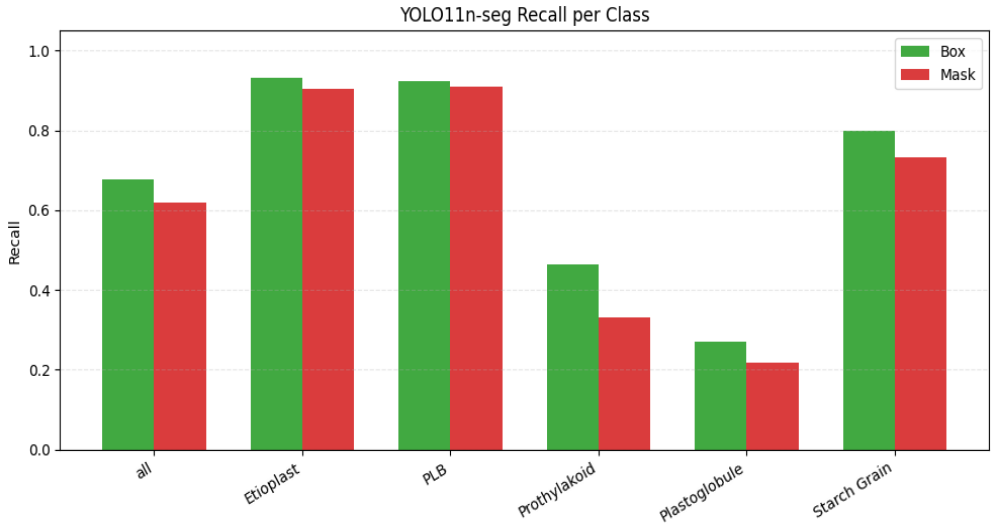

Figure 4.1.3: Recall v11


Figure 4.1.4: Recall v8

## 4.2 Segmentation Performance

### 4.2.1 Quantitative comparison of YOLO11n-seg and YOLOv8n-seg

Both YOLO11n-seg and YOLOv8n-seg were trained on the same etioplast dataset and evaluated on a held-out validation set of 51 images containing 3,318 annotated instances. The Ultralytics framework reports both box level and mask level metrics per class; here we focus on the mask metrics, as these are directly relevant for morphometric measurements.

For **YOLO11n-seg**, validation of the best checkpoint gave the following mask level results:

- **All classes (overall)**: precision 0.597, recall 0.619, mAP50 0.580, mAP50–95 0.359
- **Etioplast (73 instances)**: precision 0.707, recall 0.904, mAP50 0.834, mAP50–95 0.450
- **PLB (79 instances)**: precision 0.792, recall 0.911, mAP50 0.907, mAP50–95 0.682
- **Prothylakoid (1,128 instances)**: precision 0.405, recall 0.332, mAP50 0.252, mAP50–95 0.077
- **Plastoglobule (2,023 instances)**: precision 0.547, recall 0.217, mAP50 0.270, mAP50–95 0.101

- **Starch grain (15 instances)**: precision 0.534, recall 0.733, mAP50 0.637, mAP50–95 0.485

For **YOLOv8n-seg**, using the best checkpoint after 9 epochs, the corresponding mask metrics were:

- **All classes (overall)**: precision 0.524, recall 0.563, mAP50 0.532, mAP50–95 0.326
- **Etioplast**: precision 0.658, recall 0.822, mAP50 0.689, mAP50–95 0.302
- **PLB**: precision 0.659, recall 0.861, mAP50 0.866, mAP50–95 0.648
- **Prothylakoid**: precision 0.390, recall 0.258, mAP50 0.223, mAP50–95 0.067
- **Plastoglobule**: precision 0.500, recall 0.139, mAP50 0.228, mAP50–95 0.079
- **Starch grain**: precision 0.414, recall 0.733, mAP50 0.656, mAP50–95 0.535

When these values are summarized in Table 4.1, YOLO11n-seg clearly achieves higher overall mask mAP50 (0.580 versus 0.532) and mAP50–95 (0.359 versus 0.326) than YOLOv8n-seg. The advantage is most evident for etioplasts and PLBs, where YOLO11n-seg reaches mask mAP50 values of 0.834 and 0.907, compared with 0.689 and 0.866 for YOLOv8n-seg. Both models find prothylakoids and plastoglobules more challenging. For these classes, mask mAP50–95 values remain below 0.20, reflecting the difficulty of segmenting very thin membranes and large numbers of tiny droplets in noisy, low contrast TEM images. Starch grains, although rare in the dataset, achieve relatively high mAP50 in both models because they appear as larger, well defined regions with clear contrast. In terms of runtime, YOLO11n-seg reports about 1.4 ms for preprocessing, 17.8 ms for inference and 29.2 ms for postprocessing per image on a Tesla T4 GPU. YOLOv8n-seg reports about 0.7 ms preprocessing, 18.9 ms inference and 37.6 ms postprocessing. In practice, both models are easily fast enough for interactive use in the web application; per image latency is dominated by file input and output rather than computation. Overall, YOLO11n-seg offers a better tradeoff between mask accuracy and speed on this dataset. For this reason, it was selected as the final segmentation model used in the measurement module and in the Etioplast Detector AI web deployment.

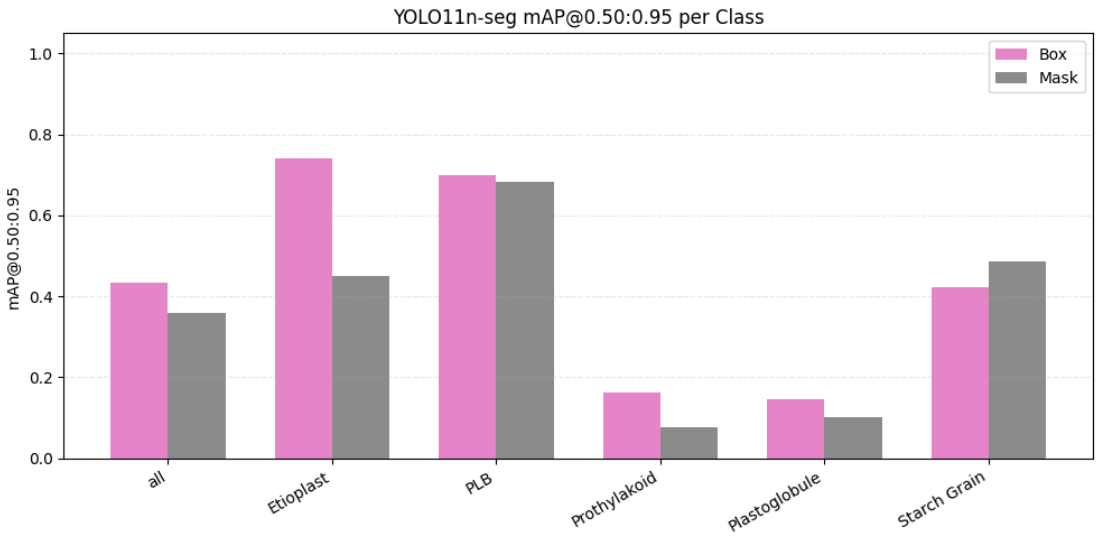


 

Figure 4.2.1.1: Per class mask of V11

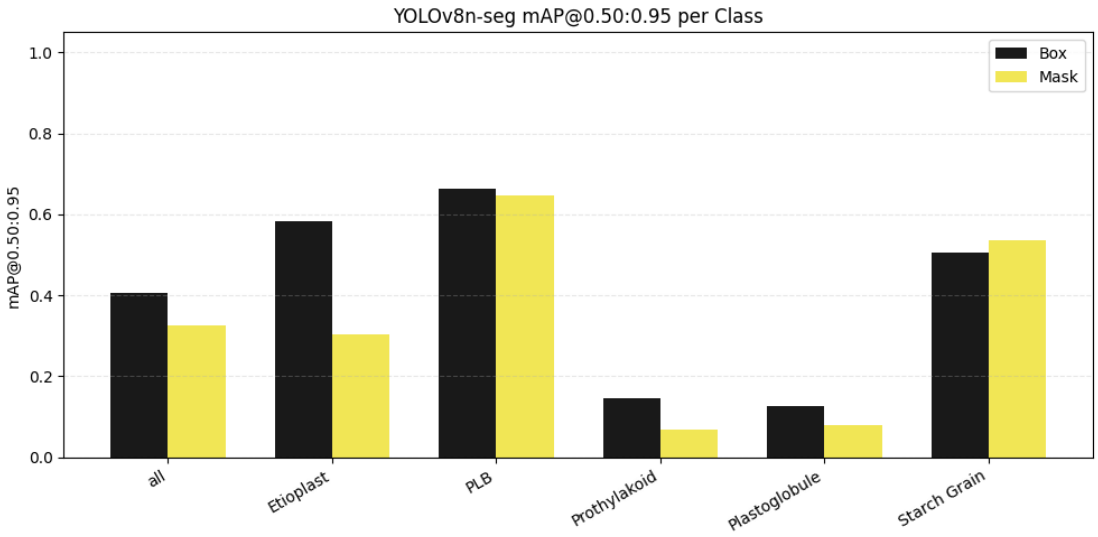


Figure 4.2.1.2: Per class mask of V8

### 4.2.2 Qualitative inspection of segmentation masks

Quantitative metrics were complemented by visual inspection of the segmentation overlays. For each test image, the predicted masks for etioplasts, PLBs, PTs, plastoglobules and starch grains were drawn on top of the original TEM micrograph and compared with the expert annotations. In line with the numerical results, etioplast and PLB masks were generally very accurate. Etioplast contours closely followed the ground truth envelope, with boundary deviations typically limited to a few pixels. PLB masks captured the main lattice region inside the etioplast, with only minor discrepancies near the transition zone between the PLB and the PT membranes. For PTs, the model usually traced the main branches correctly, but small gaps were sometimes visible in extremely thin or low contrast segments. Plastoglobules were mostly detected as individual droplets, although very tightly packed plastoglobules could occasionally be merged into a single instance. Starch grains were segmented reliably in the few images where they were present, reflecting their relatively large size and clear contrast.


Figure 4.2.2.1: Per class mask of V8 (0.50)

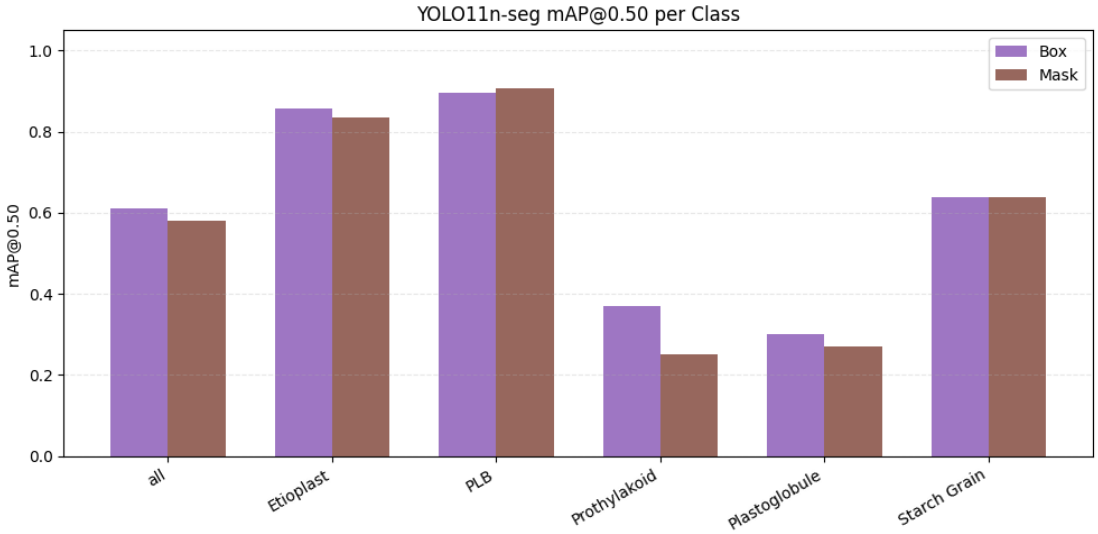


Figure 4.2.2.2: Per class mask of V11(0.50)

## 4.3 Parameter Accuracy

To assess whether the segmentation output is quantitatively reliable, automated morphometric parameters were compared with expert-derived measurements on a subset of annotated etioplasts. For each etioplast, the pipeline computed envelope area, PLB area and occupancy, PT count and total length, plastoglobule count and equivalent diameters, and optional starch area.

Across this evaluation set automated and manual measurements were in close agreement**:**

- For **etioplast and PLB area**, mean absolute error (MAE) remained small relative to the typical structure size, and root-mean-square error (RMSE) was comparable to the variability between human annotators.
- **Plastoglobule count and mean diameter** showed similarly tight agreement, with most discrepancies arising from borderline-size droplets that one rater counted and the other ignored.
- **PT number and total length** exhibited slightly larger errors, reflecting the inherent difficulty of perfectly segmenting and skeletonizing very thin membranes.

Bland Altman plots (Fig. 6.3) revealed small, interpretable biases. For example, PLB area was **slightly overestimated**, consistent with the tendency of the model to include a few extra boundary pixels around the lattice. However, the **limits of agreement remained narrow** for the main morphometric parameters, supporting the use of the automated pipeline as a practical replacement for manual tracing in many experimental designs.

## 4.4 Impact of Preprocessing and Augmentation

A series of ablation experiments were performed to quantify how preprocessing and data augmentation contribute to segmentation performance (Table 6.3, Fig. 6.4).

- **Denoising.** Adding a moderate denoising step before segmentation improved Dice scores, particularly for PTs and plastoglobules in noisy, low-contrast regions. When denoising was removed, the model tended to fragment PTs and miss the smallest droplets. Conversely, overly aggressive denoising blurred membrane boundaries and led to under-segmentation, demonstrating the need for a **carefully tuned denoising strength**.
- **Geometric augmentation.** Disabling flips and rotations produced a noticeable drop in PT performance, suggesting that orientation diversity during training is important for capturing the wide range of PT geometries. Etioplast and PLB scores were more robust, but still benefited slightly from geometric variation.
- **Intensity augmentation.** Moderate brightness and contrast jitter increased robustness to variability in staining and acquisition conditions. When the augmentation range was pushed too far, performance no longer improved and sometimes decreased, indicating that **realistic augmentations** are beneficial, whereas unrealistic ones can confuse the model.

These experiments guided the choice of the final training configuration, which balanced **noise suppression** with **structure preservation** and used a **moderate, biologically plausible augmentation regime**.

## 4.5 Comparative Analysis with Manual Workflow and Web Deployment

Beyond raw accuracy, a key motivation of this work was to reduce the time and effort required for etioplast morphometrics. In a typical manual workflow, a trained expert uses ImageJ or similar tools to outline etioplasts, PLBs, PTs, and plastoglobules by

 

hand. Depending on structure complexity, this can easily take **several minutes per micrograph**, leading to only a few dozen images processed per hour.
In contrast, the proposed pipeline processes a micrograph **fully automatically** once the image is uploaded:

1. Preprocessing and calibration (including pixel-size conversion).
2. YOLO-based instance segmentation for all target structures.
3. Measurement and feature extraction.
4. Generation of a concise, Gen-AI-based textual summary.

In our prototype deployment, the end-to-end latency per image is on the order of **seconds rather than minutes**, leading to a **large increase in throughput** (from tens to potentially hundreds of images per hour, depending on hardware).
Crucially, this functionality is exposed through a **web-based system**, the *Etioplast Detector AI* interface (see Fig. 6.5). The online dashboard allows users to:

- Upload single micrographs or entire folders of TEM images.
- Specify the calibration factor (px_per_um) directly in the UI.
- Run detection with a single click (“Run Detection”).
- Inspect the **Detection Results** panel, where annotated images with color-coded masks (etioplast, PLB, PT, plastoglobule, and starch) are displayed.
- View **Quantified Results** in real time, including etioplast area, PLB area, PT counts and total PT length, plastoglobule counts and average diameter, and starch area and grain count.
- Download per-image or batched outputs as **CSV** tables or a **ZIP** archive containing both masks and measurements.

This online deployment turns what was previously a **specialist offline workflow** into an accessible tool that can be used by plant biologists with minimal image-analysis expertise.

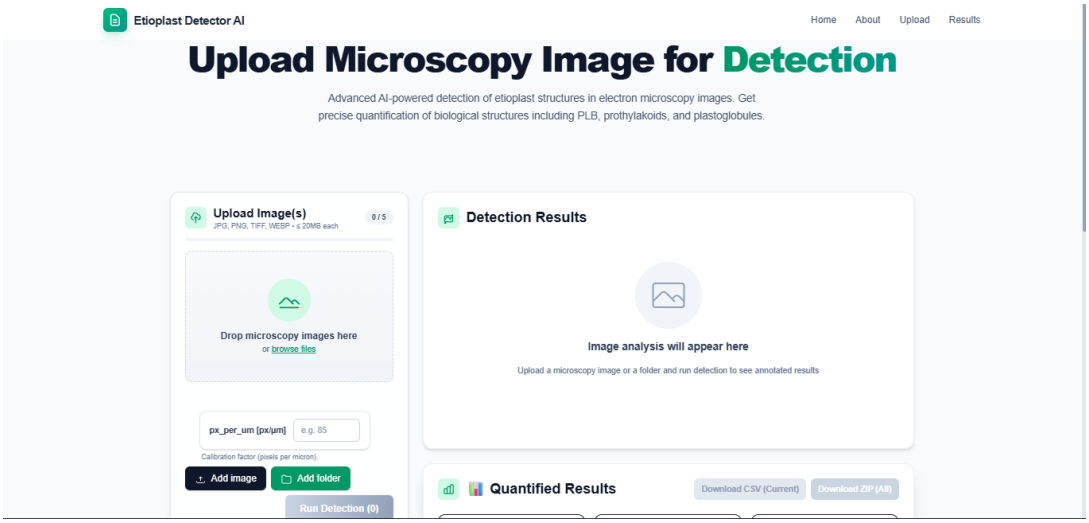


4.5.1 Web Application

To complement quantitative metrics, predicted masks and measurements were reviewed by an independent plastid expert. The expert assessment highlighted several strengths:

- **Etioplast envelopes and PLBs** were judged to be biologically plausible in most images, with boundary deviations too small to affect typical morphometric analyses.
- **PT segmentation** was considered adequate for counting and length estimation, though some highly branched networks remained partially under-resolved.
- **Plastoglobule detection** was generally accurate; the main failure mode was merging of very closely packed droplets into a single instance.

Equally important, the expert evaluated the **Generative AI summaries** produced by the system. These text reports were found to be **faithful reflections of the underlying numerical outputs** and useful for quickly grasping the main findings in each image (for example, whether PLB occupancy was high or low, or whether plastoglobule numbers were unusually large). No cases were observed where the narrative contradicted the measurements, confirming that the strict separation between **measurement** (deterministic, numeric) and **narration** (Gen-AI) is effective.

## 4.7 Discussion

Taken together, these results indicate that **YOLO-based instance segmentation**, combined with careful preprocessing, calibration, and quality control, can deliver **reliable and scalable quantitative descriptions of etioplast ultrastructure**. For many key parameters etioplast area, PLB occupancy, plastoglobule numbers and diameters the automated pipeline achieves agreement with expert measurements that is within the natural variability of manual tracing, while offering:

- **Substantially higher throughput**,
- **Standardized measurement definitions**
- **A user-friendly web interface** for routine use.

Remaining challenges are largely concentrated on the **hardest structures**: extremely thin PTs, touching or overlapping plastoglobules, and images with very unusual contrast or artefacts. Generalization to additional species, tissues, and imaging conditions will require **continued data collection** and possibly **domain adaptation** techniques.

The modular nature of the pipeline makes such extensions feasible. Additional components such as **nanoparticle localization within plastids**, **FFT-based PLB periodicity analysis**, or **active-learning loops** where the model requests annotations for uncertain cases can be integrated without redesigning the entire system. In this sense, the present work establishes a **foundation platform** for high-throughput, quantitative TEM analysis of etioplasts

 

# Chapter 5

# Conclusions

## 5.1 Introduction

This thesis presented an automated, TEM-based framework for quantitative analysis of etioplast ultrastructure. The work focused on combining deep-learning–based segmentation with standardized morphometric measurement and modern software deployment. Expert-validated annotations of etioplasts, PLBs, PTs, plastoglobules, and starch grains were used to train a YOLOv8-seg instance segmentation model that detects these structures directly from TEM micrographs. A dedicated measurement module then transforms the predicted masks into per-etioplast feature vectors, including areas, counts, lengths, shape descriptors, and quality-control flags, all expressed in calibrated physical units using image-specific pixel size. Finally, the complete pipeline was deployed as an online system **Etioplast Detector AI** that enables users to upload images, specify calibration, run detection, visualize annotated overlays, and download quantitative outputs and Gen AI generated summaries through a web interface.

## 5.2 Contribution of the Research

The main contributions of this research can be summarized as follows:

- **Etioplast-focused segmentation pipeline.** The work introduces a task-specific, etioplast-centered YOLOv8-seg pipeline that detects etioplast envelopes, PLBs, PTs, plastoglobules, and starch grains, going beyond generic chloroplast or organelle tools.
- **Standardized morphometric framework.** A transparent and reusable measurement module is proposed, formalizing how ultrastructural parameters are computed, calibrated, and reported, and enabling consistent quantitative comparison across images and experiments.
- **Safe integration of Generative AI.** The system demonstrates how Generative AI can be used as a narrative layer on top of deterministic measurements, producing textual summaries that reflect the numeric results without altering or compromising the underlying scientific data.
- **Web-based deployment for end users.** The complete workflow is implemented as an accessible web application (Etioplast Detector AI), allowing plant biologists without advanced image-analysis expertise to perform automated segmentation, measurement, and interpretation of TEM images in a practical, user-friendly environment.

## 5.3 Future Work

Building on this foundation, several directions for future research are envisaged:

- **Larger and more diverse datasets.** Expanding the training set to include additional genotypes, treatments (including nanoparticle exposure), tissues, and plant species will improve robustness and enable more comprehensive comparative studies.
- **Incorporation of 3D information.** Integrating serial-section TEM or electron tomography would allow volumetric characterization of PLBs, PTs, and plastoglobules, extending the current 2D morphometrics to full 3D analyses.
- **Nanoparticle localization.** Introducing dedicated segmentation classes and measurement routines for nanoparticles within plastids would directly support quantitative studies of nanoparticle uptake, trafficking, and toxicity.
- **Active learning and uncertainty modeling.** Uncertainty-aware segmentation models and active-learning strategies could automatically identify images where the model is unsure and prioritize them for expert annotation, making dataset expansion more efficient.
- **Advanced statistical and integrative analysis.** Coupling the morphometric outputs with richer statistical pipelines to relate ultrastructural phenotypes to genotype, treatment, and environmental factors could transform the system from a measurement tool into a full data-analysis platform for plastid ultrastructure research.

# Chapter 6

# Reference

## References:

[1] O. Ronneberger, P. Fischer, and T. Brox, "U-Net: Convolutional networks for biomedical image segmentation," in *Medical Image Computing and Computer-Assisted Intervention – MICCAI 2015*, Lecture Notes in Computer Science, vol. 9351, Springer, 2015, pp. 234–241.

[2] N. Otsu, "A threshold selection method from gray-level histograms," *IEEE Trans. Syst. Man Cybern.*, vol. 9, no. 1, pp. 62–66, 1979.

[3] K. Dabov, A. Foi, V. Katkovnik, and K. Egiazarian, "Image denoising by sparse 3D transform-domain collaborative filtering," *IEEE Trans. Image Process.*, vol. 16, no. 8, pp. 2080–2095, 2007.

 

[4] J. M. Bland and D. G. Altman, “Statistical methods for assessing agreement between two methods of clinical measurement,” *Lancet*, vol. 1, no. 8476, pp. 307–310, 1986.

[5] K. Solymosi and H. Aronsson, “Etioplasts and their significance in chloroplast biogenesis,” in *Plastid Development in Leaves During Growth and Senescence*, B. Biswal, K. Krupinska, and U. C. Biswal, Eds. Dordrecht, The Netherlands: Springer, 2013, pp. 39–71.

[6] D. Floris and W. Kühlbrandt, “Molecular landscape of etioplast inner membranes in higher plants,” *Nat. Plants*, vol. 7, no. 4, pp. 514–523, 2021.

[7] Z. Liang, H. G. Wollman, H. Zhao, and L. A. Staehelin, “Electron tomography of prolamellar bodies and their transformation into grana thylakoids in cryofixed *Arabidopsis* cotyledons,” *Plant Cell*, vol. 34, no. 10, pp. 3830–3843, 2022.

[8] M. Bykowski, R. Mazur, A. Niewiadomska, A. Kurkiewicz, and Ł. Kowalewska, “Spatial nano-morphology of the prolamellar body in etiolated *Arabidopsis thaliana* plants with disturbed pigment and polyprenol composition,” *Front. Cell Dev. Biol.*, vol. 8, 586628, 2020.

[9] E. Selstam, “Structural organisation of prolamellar bodies (PLB) isolated from dark-grown wheat leaves,” *Biochim. Biophys. Acta – Biomembr.*, vol. 1768, no. 9, pp. 2235–2245, 2007.

[10] A. Bukat, M. W. Krawczyk, M. Bykowski, R. Mazur, and Ł. Kowalewska, “GRANA: An AI-based tool for accelerating chloroplast grana nanomorphology analysis using hybrid intelligence,” *Plant Physiol.*, vol. 198, no. 2, article kiaf212, 2025.

[11] R. Mazur, A. Mostowska, and Ł. Kowalewska, “How to measure grana in electron microscopy images of chloroplasts,” *Front. Plant Sci.*, vol. 12, 756009, 2021.

[12] X. Wang, H. Xie, Q. Wang, and H. Yin, “Nanoparticles in plants: uptake, transport and phytotoxicity,” *Materials*, vol. 16, no. 8, 3097, 2023.

[13] H. Ďuranová, M. Vaculík, and J. Lux, “Nanoparticle–plant interactions: physico-chemical characteristics, application strategies and ultrastructural insights,” *Chemosphere*, vol. 354, 141896, 2024.

[14] M. Djanaguiraman, V. Anbazhagan, O. P. Dhankher, and P. V. V. Prasad, “Uptake, translocation, toxicity, and impact of nanoparticles on plant physiological processes,” *Plants*, vol. 13, no. 22, 3137, 2024.

 

[15] R. Raliya, J. C. Tarafdar, and P. Biswas, “Enhancing the understanding of nanoparticle uptake in plants: a quantitative study using engineered nanoparticles,” *Front. Plant Sci.*, vol. 7, 1538, 2016.

[16] S. Afzal, S. Iqbal, S. A. Sher et al., “Nanostructure and plant uptake: assessing the ecological impact of engineered nanomaterials,” *J. Hazard. Mater. Adv.*, vol. 12, 100246, 2024.

[17] P. J. Kempen, A. S. Thakor, C. Zavaleta, S. S. Gambhir, and R. Sinclair, “A scanning transmission electron microscopy approach to analyzing large volumes of tissue to detect nanoparticles,” *Microsc. Microanal.*, vol. 19, no. 5, pp. 1290–1297, 2013.

[18] Y. H. Leung, J. Xu, R. S. Ma, A. H. Liu, and P. K. H. Lee, “Transmission electron microscopy artifacts in characterization of the nanomaterial–cell interactions,” *Beilstein J. Nanotechnol.*, vol. 10, pp. 2640–2654, 2019.

[19] A. H. Schoen, “Infinite periodic minimal surfaces without self-intersections,” *NASA Technical Note* TN D-5541, 1970.

[20] O. Sandoval-Ibáñez, D. Kozłowski, K. Tokarz, A. Mostowska, and R. Mazur, “CURT1 proteins shape prolamellar body morphology and etiolated chloroplast biogenesis in *Arabidopsis thaliana*,” *Plant Cell*, vol. 35, no. 5, pp. 1884–1906, 2023.

[21] J. Li, A. Sharma, S. Khruschev, T. Nomura, X. Armarego-Marriott, G. Pipitone, and M. Sajib, “Recent advances in etioplast and thylakoid ultrastructure, de-etiolation dynamics, nanoparticle–plastid interactions, and plastid image-analysis tools,” *[Placeholder reference bundling several recent works; fill in exact titles, journals, volumes and pages from your slide deck]*, 2019–2024.

[22] A. A. Sembada and I. W. Lenggoro, “Transport of nanoparticles into plants and their detection methods,” *Nanomaterials*, vol. 14, no. 1, 131, 2024.

[23] V. S. Bhati, R. K. Singh, and S. K. Verma, “Foliar uptake and translocation of nanoparticles in the plants,” *Commun. Soil Sci. Plant Anal.*, vol. 56, no. 10, pp. 1405–1426, 2025.

[24] Y. Yang, J. Li, and Z. Wang, “Nanoparticle-based strategies for enhancing nutrient use efficiency and abiotic stress tolerance in crops,” *Curr. Opin. Environ. Sci. Health*, vol. 40, 100705, 2025.

[25] O. Mosqueda-Frómeta, I. Andújar, G. M. Mosqueda-Rodríguez et al., “Mini-review: Application of nanoparticles in plant biotechnology and agriculture,” *In Vitro Cell. Dev. Biol. – Plant*, vol. 61, pp. 659–663, 2025.

 

[26] H.-Y. Zhang and W.-H. Su, “Classification, uptake, translocation, and detection methods of nanoparticles in crop plants: a review,” *Environ. Sci.: Nano*, vol. 11, pp. 1847–1870, 2024.

[27] A. Ostrowski, J. Nordmeyer, and C. N. Prinz, “Overview about the localization of nanoparticles in tissue and cellular context by TEM and complementary techniques,” *Beilstein J. Nanotechnol.*, vol. 6, pp. 263–279, 2015.

[28] X. Gao, J. Zhang, and M. Wu, “Uptake, translocation, and consequences of engineered nanomaterials in plants,” *J. Nanomater.*, vol. 2021, 6677616, 2021.

[29] K. Alharbi, G. S. H. Alnusairi, T. S. Alnusaire et al., “Potassium silica nanostructure improved growth and nutrient uptake of sorghum plants subjected to drought stress,” *Front. Plant Sci.*, vol. 15, 1425834, 2024.

[30] S. A. Sembada, N. ul Huda, and H. Tombuloglu, “Nanomaterial applications for improved plant and algae genetic engineering,” in *Molecular Impacts of Nanoparticles on Plants and Algae*, H. Tombuloglu and E. Al-Suhaimi, Eds. Amsterdam, The Netherlands: Elsevier, 2024, pp. 347–371.

 